Chinese Journal of Physics 69 (2021) 172–185

Contents lists available at ScienceDirect

Chinese Journal of Physics

journal homepage: www.sciencedirect.com/journal/chinese-journal-of-physics

Transportation of magnetite nanofluid flow and heat transfer over a rotating porous disk with Arrhenius activation energy: Fourth order Noumerov's method

R. Kumar [*,a], A. Bhattacharyya [b], G.S. Seth [a], Ali J. Chamkha [c,d]

[a] Department of Mathematics and Computing, Indian Institute of Technology (Indian School of Mines), Dhanbad 826004, India
[b] Department of Mathematics, GITAM School of Science, GITAM University, Bengaluru 561203, Karnataka, India
[c] Institute of Theoretical and Applied Research (ITAR), Duy Tan University, Hanoi 100000, Vietnam
[d] Institute of Research and Development, Duy Tan University, Da Nang 550000, Vietnam

ARTICLE INFO

Keywords:
Rotating porous disk
Thermophoresis
Brownian motion
Arrhenius activation energy
Fourth order Noumerov discretization

ABSTRACT

This article explains the effect of magnetite nanofluid taking into account water as the base fluid, over a rotating disk in the presence of external magnetic field. The governing boundary layer equations of laminar and incompressible flow over rotating disk have been formulated under the simultaneous influence of thermophoresis and Brownian motion. Additionally, influence of chemical reaction between species, prompted by Arrhenius activation energy is considered into the model. The Von Karman's transformations of the Navier-Stokes equations are used to obtain the non-dimensional forms of the governing equations, and then fourth order finite difference scheme is used to find the numerical solutions using Noumerov's discretization. This technique has strong impact on the accuracy of finite difference scheme. The physical descriptions of fluid velocity, temperature, concentration profiles and quantities of practical interest such as skin friction coefficient, Nusselt number and Sherwood number are presented with the help of graphs. One of the significant findings of this analysis include that an intensification in the thermophoresis parameter causes a downfall in the rate of heat transfer at the surface of the disk whereas another significant outcomes of the present investigation is that there is a downfall in the behaviours of the species concentration with the strengthening of Arrhenius activation energy. The fluid flow due to rotating disks has application in mechanisms of thermal transformations for nuclear propulsion devices.

1. Introduction

The modern nano-technology allowed the researchers to search for colloidal suspension of nanometer sized particles, called nanoparticles, in a base fluid. Nanoparticles are small sized particles used in base fluid and their suspension is termed as nanofluid. Nanofluids have numerous practical applications that make them fruitful in several areas such as heat exchanger, chiller, domestic refrigerator, microelectronics, engine cooling/vehicle thermal management, hybrid-powered engines, pharmaceutical processes and fuel cells. Nanofluids exhibit improved thermal properties as coolants in heat transport equipment, including heat exchangers, radiators and electronic cooling system(such as flat plate). Several researchers examined numerical and experimental studies to find the

* Corresponding author.
E-mail address: rajan.2015dr0119@am.iitism.ac.in (R. Kumar).

https://doi.org/10.1016/j.cjph.2020.11.018
Received 3 September 2020; Received in revised form 21 November 2020; Accepted 29 November 2020
Available online 11 December 2020

numerous possible application of nanofluids to control the heat transport in a process, due to their enhancing applications in recent years. Masuda et al. [1] first mentioned the strange improvement in the thermal conductivity of nanofluids. Using the Buongiorno model, MHD nanofluid flow with partial slip over a rotating disk was explored by Mustafa [2]. Yin et al. [3] studied the heat transfer mechanism due to the fluid flow over a stretchable rotating disk in the radial direction. Yildiz et al. [4] explained the theoretical and experimental investigation of thermal conductivity regarding the model of hybrid nanofluid i.e. $Al_2O_3 - SiO_2$ with water as base fluid. Xu [5] found the analytical solution of unsteady mixed convection nanofluid flow between two rotating disks taking into account different kinds of nanoparticles. Kumar et al. [6] analyzed the axisymmetric flow of an electrically conducting viscous nanofluid between two stretchable co-axial rotating disks in the presence of porous medium. Other useful relevant studies are due to [7–13].

The flow of nanofluids under the impact of magnetic field have numerous applications in engineering. Moving electric charge can produce magnetic field and magnetic field is that area where magnetic force can be observed around a magnet. By applying a magnetic field in the flow region, flow of nanofluid provides comprehensive explanations of the heat transport and the hydro-magnetic properties. Such studies have significant applications in the field of drug delivery mechanisms and micro-scale flow control in microfluidic circuits. Another use of magnetic fields in metallurgical processes is purification of molten phase of metals. Motivated by above industrial application, Pavlov [14] initiated the investigation of boundary layer flow of electrically conducting fluid due to a deforming plate. Rashidi et al. [15] discussed the analytical solution of diffusion-thermo and thermal-diffusion on steady MHD flow due to rotating porous disk under the influence of magnetic field. The influence of hydromagnetic flow between two rotating disks in the presence of magnetic field was explored by Hayat et. al [16]. The numerical investigation using (Bvp4C) based on shooting technique including thermal radiation and heat source/sink effects on nanofluid flow and heat transfer between two coaxial rotating disks was investigated by Khan et al. [17]. Based on the finite difference method, namely (Bvp4C), Ahmed et al. [18] investigated unsteady thin film flow of Maxwell nanofluid over a rotating disk using the Buongiorno model. The fluid flow and transportation via porous medium are phenomenon of practical importance in several fields like mining, chemical engineering, chemical engineering, civil engineering, hydrology and many more. Bhat and Kategi [19] explored a micropolar fluid flow between porous and non-porous disks, which was solved by Keller-box method. Hayat et al. [20] examined the steady state of three dimensional flow of Jeffrey nanofluid over a rotating disk, taking into account the influence of convective flow through a porous medium in the presence of magnetic field.

Brownian motion and thermophoresis are very significant to understand the phenomenon of heat and mass transport characteristics. Thermophoresis is noticed in the solution of mobile particles where various kinds of particles perform different responses to temperature difference. The random motion of suspended particles in fluid is known as Brownian motion. The motion occurs due to fast moving molecules or atoms which hit the particles. Migration of nanoparticles into nanofluids takes place because of the slip mechanisms, a key aspect which increases the heat transfer rate and the thermal conductivity. There are many factors which affect the slip mechanism in nanofluid flow. Out of these, the two mechanisms dominate the process of slip mechanism, which are thermophoresis and Brownian diffusion as suggested by Buongiorno [21]. Rehman et al. [22] scrutinized the Casson nanofluid flow above the rigid disk as a semi infinite region. They explored the influence of thermophoresis and Brownian motion on rotating disk with uniform angular velocity, which has been numerically solved. The simultaneous impact of both Brownian motion and thermophoresis in a transient flow between rotating porous disks has been investigated by Saidi and Tamim [23]. A numerical approach has been accomplished by Lin and Jiang [24] in order to find the influence of Brownian motion and thermophoresis due to the flow of nanofluid in a rotating circular groove. Taking into account the flow configuration of third grade nanofluid between parallel plates in a rotating system under the effect of both Brownian motion and thermophoresis was described by Shah et al. [25]. Seth et al. [26] presented Newton's linearization technique to discuss the phenomenon of entropy production over a stretching surface under the influence of both ohmic heating and viscous dissipation. Some useful research works in this regard are due to Refs. [27–35].

To initiate chemical reaction, a minimum energy is required for reaction, which is termed as activation energy. Svante Arrhenius explained the concept of activation energy in 1989. The Arrhenius equation presents the quantitative basis for the relationship between the rate at which a reaction and activation energy take place. Initially, the value of activation energy is zero in the system for chemical reaction. Activation energy is the energy a reacting molecule needs to be converted into a product. A reaction happens when this barrier is passed. According to the Maxwell distribution, those atoms pass this barrier that have a higher energy than the barrier. Therefore we consider activation energy to be the barrier height. Hayat et al. [36] studied the entropy production of Ree-Eyring nanofluid flow between two rotating disks with Arrhenius activation energy. In their model, they incorporated the semi analytic method to solve the non linear differential equations. The mechanism of entropy production on nanofluid flow over a stretching surface with activation energy was studied by Kumar et al. [37]. Khan et al. [34] discussed the mechanism of entropy production in the MHD radiative flow of nanomaterial considering second order chemical reaction, prompted by supplying activation energy.

There are number of published researched articles which deal with the importance of steady flow over a rotating disk under the influence of magnetic field. But further investigation in this regard is needed to clarify the effect of Brownian motion and thermophoresis with Arrhenius activation energy, which is the main motivation of this paper. The aim of the present work is to analyze the new aspects of the studies mentioned above. Motivated by these facts, the present model has been carried out to examine the fluid flow due to rotating porous disks under the influence of magnetic field, taking into account the Arrhenius activation energy. Influence of nanoparticle volume fraction, permeability parameter, Brownian motion parameter, magnetic parameter, thermophoresis parameter, chemical reaction parameter and activation energy are particularly emphasized in this present article. The governing boundary layer equations of laminar and incompressible flow over a rotating disk are transformed to non-linear differential equations. The Von

Karman's transformations of the Navier-Stokes equations are used to obtain the non-dimensional forms of the governing equations, and then fourth order Noumerov's method is used to find the numerical solutions. This method definitely has a strong impact on the accuracy of the solutions obtained.

2. Flow analysis

The physical model for nanofluid flow over a rotating disk is considered with the fact that the flow is steady, axially symmetric and incompressible. The rotating disk is placed at $z = 0$. Physical assumptions while modelling the flow phenomena are as follows:

- A magnetic field of uniform intensity B_0 is applied along z-direction which is normal to the surface of disk.
- Since magnetic Reynolds number is small, we ignore the influence of induced magnetic field.
- The components of the fluid velocities i.e. (u, v, w) are in directions of respective cylindrical coordinates i.e. along (r, ϑ, z) respectively. The disk rotates with an angular velocity Ω.
- The uniform temperature and concentration of the surface of the rotating disk are kept at T_w and C_w, respectively, while the pressure, temperature and concentration of the ambient nanofluid are maintained at P_∞, T_∞ and C_∞ respectively.
- Behaviors of thermophoresis and Brownian motion are taken into consideration.
- Additionally, we have carried out an analysis of mass transfer by considering binary chemical reaction, which has been stimulated by Arrhenius activation energy. The schematic diagram of the flow situation is presented in Fig. 1.

With the help of above mentioned assumptions, the governing equations of laminar and incompressible boundary layer nano-fluid flow over a rotating disk, [36,38] are given by:

$$\frac{\partial u}{\partial r} + \frac{\partial w}{\partial z} + \frac{u}{r} = 0, \tag{1}$$

$$u\frac{\partial u}{\partial r} + w\frac{\partial u}{\partial z} - \frac{v^2}{r} + \frac{1}{\rho_{nf}}\frac{\partial p}{\partial r} = \nu_{nf}\nabla^2 u - \frac{\nu_{nf}}{k^*}u - \frac{\sigma_{nf}}{\rho_{nf}}B_0^2 u, \tag{2}$$

$$u\frac{\partial v}{\partial r} + w\frac{\partial v}{\partial z} + \frac{vu}{r} = \nu_{nf}\nabla^2 v - \frac{\nu_{nf}}{k^*}v - \frac{\sigma_{nf}}{\rho_{nf}}B_0^2 v, \tag{3}$$

$$u\frac{\partial w}{\partial r} + w\frac{\partial w}{\partial z} + \frac{1}{\rho_{nf}}\frac{\partial p}{\partial z} = \nu_{nf}\nabla^2 w - \frac{\nu_{nf}}{k^*}w, \tag{4}$$

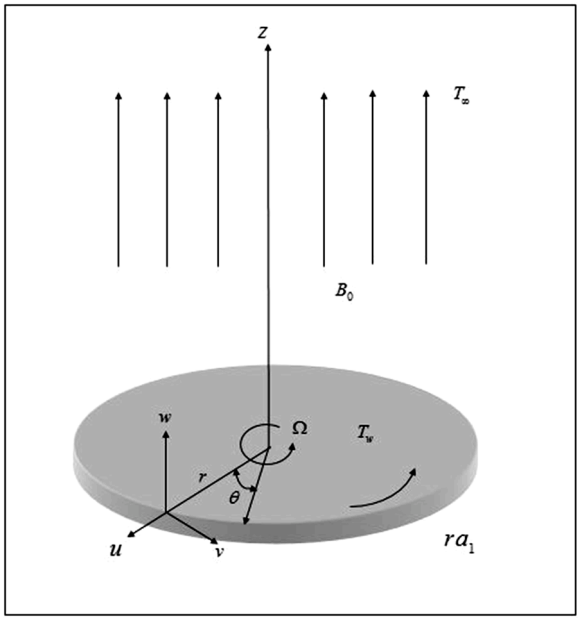

Fig. 1. Schematic diagram of the flow situation.

$$u\frac{\partial T}{\partial r}+w\frac{\partial T}{\partial z}=\alpha_{nf}\nabla^2 T+\frac{(\rho c_p)_s}{(\rho c_p)_{nf}}\left[\frac{D_T}{T_\infty}\left(\left(\frac{\partial T}{\partial z}\right)^2+\left(\frac{\partial T}{\partial r}\right)^2\right)+D_B\left(\frac{\partial T}{\partial z}\frac{\partial C}{\partial z}+\frac{\partial T}{\partial r}\frac{\partial C}{\partial r}\right)\right], \tag{5}$$

$$u\frac{\partial C}{\partial r}+w\frac{\partial C}{\partial z}=D_B\nabla^2 C+\frac{D_T}{T_\infty}\nabla^2 T-k_r^2\left(\frac{T}{T_\infty}\right)^n\exp\left[\frac{-E_a}{kT}\right]\left(C-C_\infty\right), \tag{6}$$

where T is the temperature, C is the concentration, p is the pressure, α_{nf} is the thermal diffusivity of the nanofluids, ν_{nf} is the kinematic viscosity of the nanofluids, α_{nf} is the thermal diffusivity of the nanofluids, $(\rho c_p)_{nf}$ is the specific heat capacity of nanofluids, D_T is the thermophoretic diffusion coefficient, D_B is the Brownian diffusion coefficient, k^* is the permeability of porous medium, ρ_{nf} is the density of the nanofluids, k_r is the reaction rate, E_a is the activation energy and $\left(\frac{T}{T_\infty}\right)^n\exp\left[\frac{-E_a}{kT}\right]$ is the Arrhenius function.

For nanofluids, the expressions of ν_{nf}, α_{nf}, μ_{nf}, ρ_{nf}, $(\rho c_p)_{nf}$ and σ_{nf} are defined as $\nu_{nf}=\frac{\mu_{nf}}{\rho_{nf}}$, $\alpha_{nf}=\frac{k_{nf}}{(\rho c_p)_{nf}}$, $\mu_{nf}=\frac{\mu_f}{(1-\phi)^{2.5}}$, $\rho_{nf}=\rho_f(1-\phi)+\rho_s\phi$, $(\rho c_p)_{nf}=(\rho c_p)_s\phi+(\rho c_p)_f(1-\phi)$, $k_{nf}=k_f\left[\frac{(k_s+2k_f)-2\phi(k_f-k_s)}{(k_s+2k_f)+\phi(k_f-k_s)}\right]$ and $\sigma_{nf}=\sigma_f\left[1+\frac{3(\sigma_s/\sigma_f-1)\phi}{(\sigma_s/\sigma_f+2)-(\sigma_s/\sigma_f-1)\phi}\right]$, where ϕ is the solid volume fraction of the nanoparticles, k_s is the thermal conductivity of the nanoparticles, k_f is the thermal conductivity of base fluid, ρ_s and ρ_f are the density of the nanoparticles and base fluid respectively, $(\rho c_p)_f$ is the heat capacitance of the base fluid, μ_f is the viscosity of the base fluid, σ_{nf} is the electrical conductivity and $(\rho c_p)_s$ is the heat capacitance of the nanoparticles. The thermophysical characteristics of magnetite and water are given in Table 1.

The thermal and hydrodynamic boundary conditions subject to uniform suction w_0 through the disk for the governing boundary layer equations are

$$\begin{aligned} &u=0, v=r\Omega, w=w_0, T=T_w, C=C_w, && \text{at} \quad z=0,\\ &u\to 0, v\to 0, P\to P_\infty, T\to T_\infty, C\to C_\infty, && \text{at} \quad z\to\infty, \end{aligned} \tag{7}$$

The Von Karman's transformations of the Navier-Stokes equations are used to obtain the non-dimensional forms

$$\begin{aligned} &\zeta=z\left(\frac{\Omega}{\nu_f}\right)^{1/2},\quad u=r\Omega f(\zeta),\quad v=r\Omega g(\zeta),\quad w=\left(\Omega\nu_f\right)^{1/2}h(\zeta)\\ &p-p_\infty=2\mu_f\Omega p(\zeta),\quad \theta=\frac{T-T_\infty}{T_w-T_\infty},\quad \phi=\frac{C-C_\infty}{C_w-C_\infty}. \end{aligned} \tag{8}$$

After using the transformations (8), we are seeking a similar solutions of governing Eqs. take the following non-dimensional form

$$2f(\zeta)+h'(\zeta)=0, \tag{9}$$

$$E_1\left(f''(\zeta)-\lambda f(\zeta)\right)-h(\zeta)f'(\zeta)-f^2(\zeta)+g^2(\zeta)-E_2Mf(\zeta)=0, \tag{10}$$

$$E_1(g''(\zeta)-\lambda g(\zeta))-E_2Mg(\zeta)-2f(\zeta)g(\zeta)-h(\zeta)g'(\zeta)=0, \tag{11}$$

$$2E_2\frac{\sigma_f}{\sigma_{nf}}P'(\zeta)+h(\zeta)h'(\zeta)-E_1h''(\zeta)+\lambda E_1h(\zeta)=0, \tag{12}$$

$$\frac{1}{Pr}E_3\theta''(\zeta)-h(\zeta)\theta'(\zeta)+Nb\theta'(\zeta)\varphi'(\zeta)+Nt\theta'^2(\zeta)=0, \tag{13}$$

$$\frac{1}{S_c}\varphi''(\zeta)-h(\zeta)\varphi'(\zeta)+\frac{1}{S_c}\frac{Nt}{Nb}\theta''(\zeta)-\gamma(1-\theta\theta_w)^m\exp\left[\frac{E}{(1+\theta\theta_w)}\right]=0, \tag{14}$$

where $E_1=\frac{1}{(1-\phi)^{2.5}\left(1-\phi+\frac{\rho_s}{\rho_f}\phi\right)}$, $E_2=\frac{1}{\left(1-\phi+\frac{\rho_s}{\rho_f}\phi\right)}\frac{\sigma_{nf}}{\sigma_f}$ and $E_3=\frac{k_{nf}}{k_f}\frac{(\rho c_p)_f}{(\rho c_p)_{nf}}$.

The boundary conditions associated with the non-dimensional governing equations are given as

Table 1
Thermophysical features of Fe_3O_4 and H_2O [39].

	k(W/mK)	C_p(J/kgk)	$\sigma(\mathrm{Um})^{-1}$	ρ(Kg/m^3)
H_2O	0.613	4179	0.05	997.1
Fe_3O_4	9.7	670	25,000	5180

$$f(0)=0,\quad g(0)=1\quad h(0)=W_s,\quad \theta(0)=1,\quad \varphi(0)=1,$$
$$f(\zeta)\to 0,\ g(\zeta)\to 0,\ \theta(\zeta)\to 0,\ \varphi(\zeta)\to 0\quad as\quad \zeta\to\infty. \tag{15}$$

where $Pr=\frac{\nu_f(\rho C_p)_f}{k_f}$ is the Prandtl number, $M=\frac{\sigma_f B_0^2}{\Omega\rho_f}$ is the magnetic parameter, $\lambda=\frac{\nu_f}{k^*\Omega}$ is the porosity parameter, $N_b=\frac{(C_w-C_\infty)D_B}{\nu_f}\frac{(\rho C_p)_s}{(\rho C_p)_{nf}}$ is the Brownian motion parameter, $N_t=\frac{(T_w-T_\infty)D_T}{\nu_f}\frac{(\rho C_p)_s}{(\rho C_p)_{nf}}$ is the thermophoresis parameter, $S_c=\frac{\nu_f}{D_B}$ is the Schmidt number, $\theta_w=\frac{T_w-T_\infty}{T_\infty}$ is the temperature difference parameter, W_s is the suction/injection parameter, $E=\frac{-E_a}{KT_\infty}$ is the activation energy and $\gamma=\frac{k_c^2}{\Omega}$ is the chemical reaction rate.

3. Physical quantities

The **skin friction coefficients** at the surface of the disk is represented by the mathematical expression C_f as

$$C_f=\frac{\sqrt{\tau_{w\phi}^2+\tau_{wr}^2}}{\rho_f(r\Omega)^2}=\frac{1}{Re^{1/2}(1-\phi)^{5/2}}\sqrt{\left[(f'(0))^2+(g'(0))+\right]}, \tag{16}$$

where $\tau_{w\phi}$ and τ_{wr} are the transversal and radial shear stress at the surface of the disk, respectively, and $Re=\frac{\Omega r^2}{\nu_f}$ is Reynolds number. The expression of $\tau_{w\phi}$ and τ_{wr} are defined as

$$\tau_{w\phi}=\mu_{nf}\left(\frac{\partial v}{\partial z}+\frac{1}{r}\frac{\partial w}{\partial\phi}\right)\Big|_{z=0},\quad \tau_{wr}=\mu_{nf}\left(\frac{\partial u}{\partial z}+\frac{\partial w}{\partial\phi}\right)\Big|_{z=0}. \tag{17}$$

The **Nusselt number** has been calculated at surface of disk which measures the rate of heat transfer and it is denoted by Nu as

$$Nu=\frac{rq_w}{k_f(T_w-T_\infty)}\Big|_{z=0}=-\frac{1}{Re^{-1/2}}\frac{k_{nf}}{k_f}\theta'(0), \tag{18}$$

where q_w is heat flux which is given as

$$q_w|_{z=0}=-k_{nf}\frac{\partial T}{\partial z}\Big|_{z=0}. \tag{19}$$

The **Sherwood number** at the surface of the disk is represented by the mathematical expression Sh as:

$$Sh=\frac{rq_m}{D_B(C_w-C_\infty)}\Big|_{z=0}=-\varphi'(0), \tag{20}$$

where q_m is expressed as
$q_m = -D_B\frac{\partial C}{\partial z}$.

4. Numerical procedure

The coupled non-linear ordinary differential Eqs. (9)-(14) along with boundary conditions (15) have been solved numerically. Fourth order finite difference scheme is implemented to solve the non-linear differential equations. We are now ready to convert the differential equation along with boundary conditions into the form of difference equations by introducing the expression of central difference scheme. The obtained discretized equations form a non-linear tridiagonal system of equations. The Newton's linearization technique is used to solve the non-linear system of equations after implementing the Noumerov's discretization into the differential equations. This method definitely has strong impact on the accuracy of finite difference scheme which provides the approximate numerical solutions of differential Eqs. (9)-(14)).

We are going to solve Eq. (10) and we have

$$E_1f'''(\zeta)=E_1\lambda f(\zeta)+f^2(\zeta)+h(\zeta)f'(\zeta)-g^2(\zeta)+E_2Mf(\zeta)=F\left(\zeta,f(\zeta),f'(\zeta)\right), \tag{21}$$

where $F(\zeta,f(\zeta),f'(\zeta))$ is non linear function of $f(\zeta)$ and $f'(\zeta)$, in general.

Fourth order finite difference scheme, first proposed by Noumerov[40] is a numerical technique to solve the differential Eqs. (9)-(14).

The Noumerov discretization at each internal grid point for the non-linear ODE (21) is given as [41,42]

$$E_1\left(f_{j-1}-2f_j+f_{j+1}\right)=\frac{(\delta\zeta)^2}{12}\left(\overline{F}_{j-1}+10\widehat{F}_j+\overline{F}_{j+1}\right), \tag{22}$$

where

$$\overline{F}_{j-1} = F\left(\zeta_{j-1}, f_{j-1}, \overline{f'}_{j-1}\right),$$
$$\overline{F}_{j+1} = F\left(\zeta_{j+1}, f_{j+1}, \overline{f'}_{j+1}\right),$$
$$\widehat{F}_{j} = F\left(\zeta_{j}, f_{j}, \widehat{f'}_{j}\right),$$
$$\overline{f'}_{j} = \left(f_{j+1} - f_{j-1}\right)/(2\delta\zeta),$$
$$\overline{f'}_{j+1} = \left(3f_{j+1} - 4f_{j} + f_{j-1}\right)/(2\delta\zeta),$$
$$\overline{f'}_{j-1} = \left(-f_{j+1} + 4f_{j} - 3f_{j-1}\right)/(2\delta\zeta),$$
$$\widehat{f'}_{j} = \overline{f'}_{j} - \frac{\delta\zeta}{20}\left(\overline{F}_{j+1} - \overline{F}_{j-1}\right).$$

Now, Eq. (22) becomes

$$\overline{S}_j(f_1, f_2, f_{L-1}) = P_j f_{j-1} - Q_j f_j + R_j f_{j+1} + \frac{1}{12}\left(\delta\zeta^2 g_{j-1}^2 + 5\delta\zeta^2 g_j^2 + \delta\zeta^2 g_{j+1}^2\right) = 0,\ j = 1, 2, 3 \ldots L-1, \tag{23}$$

where

$$P_j = \left(E_1 - \frac{1}{12}\delta\zeta^2 E_1\lambda - \frac{1}{12}\delta\zeta^2 f_{j-1} + \frac{1}{8}\delta\zeta h_{j-1} - \frac{1}{12}E_2 M\delta\zeta^2 + \frac{1}{12}\delta\zeta^2 h_j + \frac{5}{12}\delta\zeta h_j - \frac{1}{24}\delta\zeta h_{j-1}\right)$$
$$Q_j = \left(2E_1 + \frac{1}{6}\delta\zeta h_{j-1} + \frac{5}{6}\delta\zeta^2 E_1\lambda + \frac{5}{6}\delta\zeta^2 f_j + \frac{1}{6}\delta\zeta^2 h_j + \frac{5}{6}\delta\zeta^2 E_2 M - \frac{1}{6}\delta\zeta h_{j+1}\right)$$
$$R_j = \left(E_1 + \frac{1}{24}\delta\zeta h_{j-1} - \frac{5}{12}\delta\zeta h_j + \frac{1}{16}\delta\zeta^2 h_j + \frac{1}{48}\delta\zeta^2 h_j - \frac{1}{12}\delta\zeta^2 E_1\lambda - \frac{1}{8}\delta\zeta h_{j+1} - \frac{1}{12}\delta\zeta^2 f_{j+1} - \frac{1}{12}\delta\zeta^2 E_2 M\right)$$

$$For\ \ j = 1 : \overline{S}_1 = P_1 f_0 - Q_1 f_1 + R_1 f_2 + \frac{1}{12}\left(\delta\zeta^2 g_0^2 + 5\delta\zeta^2 g_1^2 + \delta\zeta^2 g_2^2\right) = 0,$$

$$For\ \ j = 2 : \overline{S}_2 = P_2 f_1 - Q_2 f_2 + R_2 f_3 + \frac{1}{12}\left(\delta\zeta^2 g_1^2 + 5\delta\zeta^2 g_2^2 + \delta\zeta^2 g_3^2\right) = 0,$$

$$For\ \ j = 3 : \overline{S}_3 = P_3 f_2 - Q_3 f_3 + R_3 f_4 + \frac{1}{12}\left(\delta\zeta^2 g_2^2 + 5\delta\zeta^2 g_3^2 + \delta\zeta^2 g_4^2\right) = 0,$$

$$\ldots.$$

$$\ldots.$$

$$For\ \ j = L-1 : \overline{S}_{L-1} = P_{L-1} f_{L-2} - Q_{L-1} f_{L-1} + R_{L-1} f_L + \frac{1}{12}\left(\delta\zeta^2 g_{L-2}^2 + 5\delta\zeta^2 g_{L-1}^2 + \delta\zeta^2 g_L^2\right) = 0,$$

The Jacobian of $\overline{S_j}(f_1, f_2, f_3 \ldots f_{L-1})$ is the tridiagonal matrix

$$J\left(f_j^n\right)\Delta f_j^n = \begin{bmatrix} \frac{\partial\overline{S}_1}{\partial f_1} & \frac{\partial\overline{S}_1}{\partial f_2} & 0 & \ldots & \ldots. \\ \frac{\partial\overline{S}_2}{\partial f_1} & \frac{\partial\overline{S}_2}{\partial f_2} & \frac{\partial\overline{S}_2}{\partial f_3} & 0 & \ldots \\ 0 & \frac{\partial\overline{S}_3}{\partial f_2} & \frac{\partial\overline{S}_3}{\partial f_3} & \frac{\partial\overline{S}_3}{\partial f_4} & \ldots \\ \ldots & \ldots & \ldots & \ldots & \ldots \\ 0 & \ldots & \ldots & \frac{\partial\overline{S}_{L-1}}{\partial f_{L-2}} & \frac{\partial\overline{S}_{L-1}}{\partial f_{L-1}} \end{bmatrix} \begin{bmatrix} \Delta f_1^n \\ \Delta f_2^n \\ \ldots \\ \ldots \\ \Delta f_{L-1}^n \end{bmatrix}$$

In Newton's method of lineraization, the value $f^{[1]} = f^{[0]} + \Delta f$ is accepted as a better approximation and the process is then continued if necessary, taking a suitable initial estimate $f^{[0]}$, we define

$$f_j^{[n+1]} = f_j^{[n]} + \Delta f_j^{[n]}, \quad n = 0, 1, 2, \ldots \qquad j = 1, 2, 3 \ldots L-1 \tag{24}$$

where $\Delta f_j^{[n]}$ is the solution of

$$J\left(f_j^n\right)\Delta f_j^n = a_j \Delta f_{j-1}^{n+1} + b_j \Delta f_j^{n+1} + c_j \Delta f_{j+1}^{n+1} = -f_j^n, \quad \text{for } j = 1, 2, 3 \ldots L-1, \tag{25}$$

where $j = 0$ and $j = L$ are points at the boundary. Since the solutions at $j = 0$ and $j = L$ as $f(L) = 0$ and $f(0) = 0$ are known, Δf_j^{n+1} at $j = 0$ and $j = L$ are zero. The expressions for a_j, b_j, c_j and f_j in Eq. (25) are given

$$a_j = E_1 - \frac{1}{12}\delta\zeta^2 E_1\lambda - \frac{1}{6}\delta\zeta^2 f_{j-1}^n + \frac{1}{8}\delta\zeta h_{j-1}^n - \frac{1}{12}E_2 M\delta\zeta^2 + \frac{1}{12}\delta\zeta^2 h_j^n + \frac{5}{12}\delta\zeta h_j^n - \frac{1}{24}\delta\zeta h_{j-1}^n, \tag{26}$$

$$b_j = -2E_1 - \frac{1}{6}\delta\zeta h_{j-1}^n - \frac{5}{6}\delta\zeta^2 E_1\lambda - \frac{5}{3}\delta\zeta^2 f_j^n - \frac{1}{6}\delta\zeta^2 h_j^n - \frac{5}{6}\delta\zeta^2 E_2 M + \frac{1}{6}\delta\zeta h_{j+1}^n, \tag{27}$$

$$\begin{aligned} c_j = {} & E_1 + \frac{1}{24}\delta\zeta h_{j-1}^n - \frac{5}{12}\delta\zeta h_j^n + \frac{1}{16}\delta\zeta^2 h_j^n + \frac{1}{48}\delta\zeta^2 h_j^n - \frac{1}{12}\delta\zeta^2 E_1\lambda - \frac{1}{8}\delta\zeta h_{j+1}^n - \frac{1}{6}\delta\zeta^2 f_{j+1}^n \\ & - \frac{1}{12}\delta\zeta^2 E_2 M \end{aligned} \tag{28}$$

$$\begin{aligned} f_j = {} & \left(E_1 - \frac{1}{12}\delta\zeta^2 E_1\lambda - \frac{1}{12}\delta\zeta^2 f_{j-1}^n + \frac{1}{8}\delta\zeta h_{j-1}^n - \frac{1}{12}E_2 M\delta\zeta^2 + \frac{1}{12}\delta\zeta^2 h_j^n + \frac{5}{12}\delta\zeta h_j^n - \frac{1}{24}\delta\zeta h_{j-1}^n\right) f_{j-1}^n \\ & - \left(2E_1 + \frac{1}{6}\delta\zeta h_{j-1}^n + \frac{5}{6}\delta\zeta^2 E_1\lambda + \frac{5}{6}\delta\zeta^2 f_j^n + \frac{1}{6}\delta\zeta^2 h_j^n + \frac{5}{6}\delta\zeta^2 E_2 M - \frac{1}{6}\delta\zeta h_{j+1}^n\right) f_j^n \\ & + \left(E_1 + \frac{1}{24}\delta\zeta h_{j-1}^n - \frac{5}{12}\delta\zeta h_j^n + \frac{1}{16}\delta\zeta^2 h_j^n + \frac{1}{48}\delta\zeta^2 h_j^n - \frac{1}{12}\delta\zeta^2 E_1\lambda - \frac{1}{8}\delta\zeta h_{j+1}^n - \frac{1}{12}\delta\zeta^2 f_{j+1}^n \right. \\ & \left. - \frac{1}{12}\delta\zeta^2 E_2 M\right) f_{j+1}^n + \frac{1}{12}\left(\delta\zeta^2\left(g_{j-1}^n\right)^2 + 5\delta\zeta^2\left(g_j^n\right)^2 + \delta\zeta^2\left(g_{j+1}^n\right)^2\right) \end{aligned} \tag{29}$$

The solution is modified by (24), once we obtain Δf_j^n. Now discretization of expression $h'' = -2f'$ using central difference approximation leads to solution of h employing Thomas algorithm,

$$h_{j-1}^{n+1} - 2h_j^{n+1} + h_{j+1}^{n+1} = -\delta\zeta\left(f_{j+1}^{n+1} - f_{j-1}^{n+1}\right) \tag{30}$$

The other nonlinear differential Eqs. (11)-(14) have been solved as discussed earlier. The uniform length $\delta\zeta = 0.004$ has been considered in ζ direction throughout the numerical calculation. The decrement in grid size does not affect the accuracy of the solution. In addition, the entire process can be terminated if we have found error limits maximum upto $|f_j^{n+1} - f_j^n| < 10^{-8}, \forall j$.

5. Validation of numerical results

We employed fourth order finite difference scheme, first proposed by Noumerov, which is a numerical technique for solving differential equations. The Newton's linearization technique is used to solve the non-linear system of equations after implementing the Noumerov's discretization into the differential equations. This technique has strong impact on the accuracy of finite difference scheme.

Table 2
Comparison of radial skin friction coefficient for variation of M and W_s by selecting $\phi = 0$, $Nb = Nt = 0$ and $\lambda = 0$.

		Turkyilmazoglu [43]	Kelson and Desseaux [44]	Present result
M	W_s	$f'(0)$	$f'(0)$	$f'(0)$
	0		0.510233	0.510203
0	–1		0.389569	0.389517
	–2		0.242421	0.242402
	0	0.309258		0.309218
1	–1	0.251044		0.251013
	–2	0.188719		0.188702
	0	0.165703		0.165667
4	–1	0.149016		0.149002
	–2	0.129438		0.129413

Table 3
Comparison of tangential skin friction coefficient for variation of M and W_s by selecting $\phi = 0$, $Nb = Nt = 0$ and $\lambda = 0$.

		Turkyilmazoglu [43]	Kelson and Desseaux [44]	Present result
M	W_s	$-g'(0)$	$-g'(0)$	$-g'(0)$
	0		0.61592	0.61580
0	–1		1.17522	1.17502
	–2		2.03853	2.03805
	0	1.06905		1.06865
1	–1	1.65708		1.65654
	–2	2.43136		2.43102
	0	2.01027		2.01001
4	–1	2.56933		2.56899
	–2	3.24134		3.24102

Table 4
Comparison of rate of heat transfer for variation of M and W_s by selecting $\phi = 0$, $Nb = Nt = 0$, $\lambda = 0$ and $Pr = 0.71$.

		Kelson and Desseaux [44]	Present result
M	W_s	$-\theta'(0)$	$-\theta'(0)$
	0	0.32586	0.32502
0	–1	0.79305	0.79267
	–2	1.43778	1.43708

For validation of our code, the present results of radial and tangential skin friction coefficients were compared with those of Turkyilmazoglu [43] and Kelson and Desseaux [44] for M and W_s as shown in Tables 2 and 3, respectively. Moreover, the numerical values of rate of heat transfer were compared with Kelson and Desseaux [44] for M and W_s as shown in Table 4. The numerical results of present work with developed code and previously published articles are in outstanding agreement.

6. Results and discussion

Effects of different flow parameters such as suction parameter W_s, nanoparticle volume fraction ϕ, magnetic parameter M, permeability parameter λ, thermophoresis parameter Nt, Brownian motion parameter Nb, chemical reaction parameter γ and activation energy E for magnetite nano-fluid with water as base fluid, have been discussed on velocity, temperature and concentration profiles respectively. The physical descriptions of fluid velocity, temperature, concentration profiles and quantities of practical interest such as skin friction coefficient, Nusselt number and Sherwood number are presented with the help of graphs. The default values for emerging flow parameters are chosen as $S = -1, \lambda = 0.2, M = 1, \phi = 0.2, \gamma = 0.2, P_r = 6.2, E = 2, Nb = Nt = 0.5$ and $S_c = 0.3$. For numerical computations, the fourth order finite difference method is employed along with Newton's linearization technique, which solves our non-linear equations in a very smooth way throughout the entire program.

Velocity profiles

The variation of suction parameter on tangential, radial, and axial velocities i.e. $g(\zeta)$, $f(\zeta)$ and $h(\zeta)$, respectively, for magnetite nano-fluids are shown in Figs. 2–4. It is clear from Figs. 2–4 that an increment in the axial, radial and tangential velocities as we enhance the value of W_s in magnetite nano-fluid i.e, Fe_3O_4 nano-fluids. Figs. 5 and 6 address the variation of nanoparticle volume fraction ϕ on radial and tangential velocities for Fe_3O_4 nano-fluid. A reduction in the radial and tangential velocities occur on enhancing the values of ϕ as presented in Figs. 5 and 6. This is because the velocity boundary layer becomes thinner due to the presence of nanoparticle volume fraction. An increment in nanoparticle volume fraction leads to an enhancement in thermal conductivity, whereby a drop in the velocity profiles for both Fe_3O_4 nano-fluid is observed. Figs. 7 and 8 show the behaviour of permeability

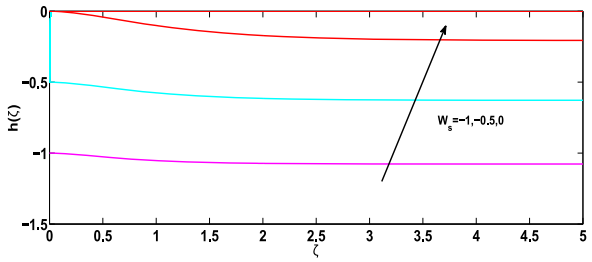

Fig. 2. Influence of W_s on axial velocity.

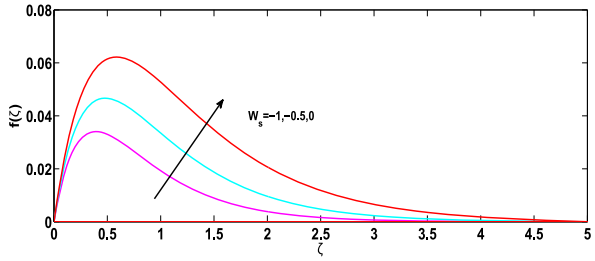

Fig. 3. Influence of W_s on radial velocity.

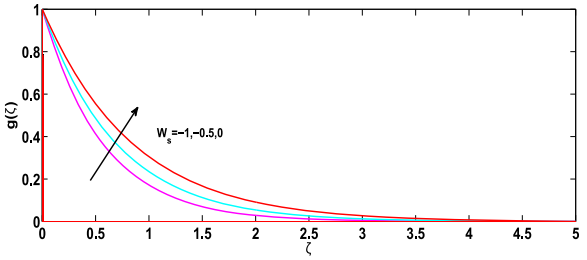

Fig. 4. Influence of W_s on tangential velocity.

parameter λ on radial and tangential velocities for magnetite nanofluid. A gradual downfall in the axial as well as radial velocities takes place while we enhance values of λ which is depicted in Figs. 7 and 8. Due to loosing the resistance of the porous medium one can observe a significant fall in the velocity profiles for Fe_3O_4 nanofluid with strengthening the porosity parameter. Effects of magnetic parameter M, on radial and tangential velocities are elucidated in Figs. 9 and 10. It is seen that with the increment in M, the radial and tangential velocities are getting decreased. The imposition of the vertical magnetic field in the electrically conductive fluid creates a drag force named as Lorentz force. This force has propensity to resist the fluid motion. As a result of which the strengthening of M leads to reduction in radial and tangential velocity profiles.

Temperature profiles

Figs. 11 and 12 describe the effects of Brownian motion parameter Nb and thermophoresis parameter Nt on temperature

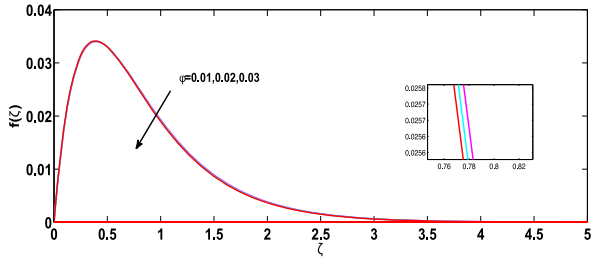

Fig. 5. Influence of ϕ on radial velocity.

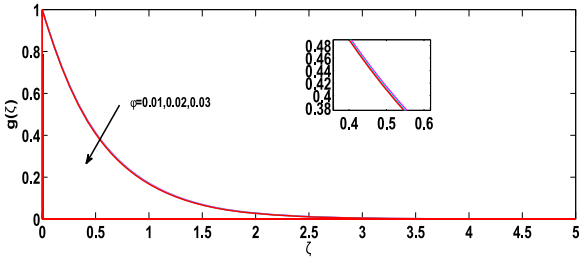

Fig. 6. Influence of ϕ on tangential velocity.

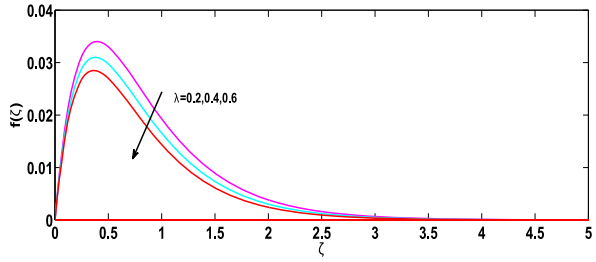

Fig. 7. Influence of λ on radial velocity.

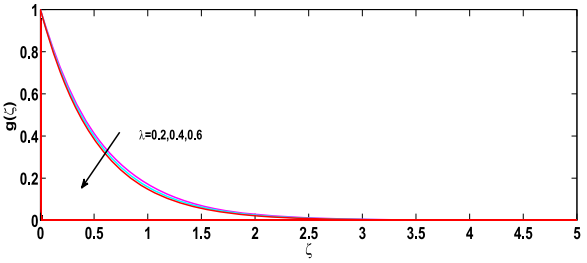

Fig. 8. Influence of λ on tangential velocity.

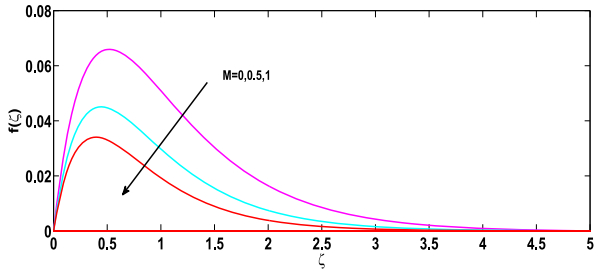

Fig. 9. Influence of M on radial velocity.

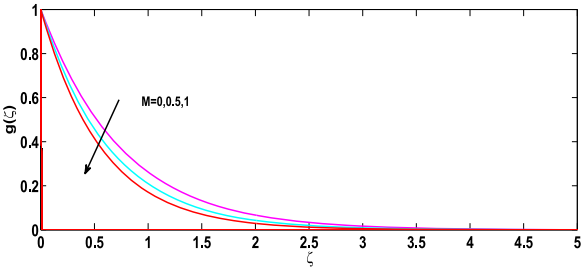

Fig. 10. Influence of M on tangential velocity.

distribution $\theta(\zeta)$, for Fe_3O_4 nano-fluid. An enhancement in the temperature profile occurs on increasing the values of Brownian motion parameter as shown in Fig. 11 for magnetite nano-fluid. Physically, an increased random motion of nanoparticles is observed due to larger values of Brownian motion parameter which results in an upsurge in the temperature distribution $\theta(\zeta)$. For Fe_3O_4 nano-fluid, the influence of thermophoresis parameter Nt is highlighted in Fig. 12. It should be noted that raising the values of thermophoresis parameter Nt leads to an increment in the temperature distribution $\theta(\zeta)$. This phenomenon can be explained with the fact that larger values of Nt results in a stronger thermophoretic force and consequently, fluid particles move from higher to lower temperature. This raises the temperature distribution $\theta(\zeta)$ for Fe_3O_4 nano-fluid.

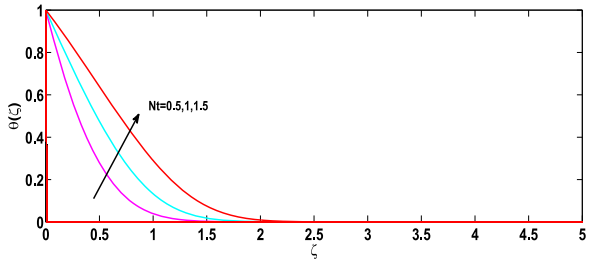

Fig. 11. Influence of *Nb* on temperature.

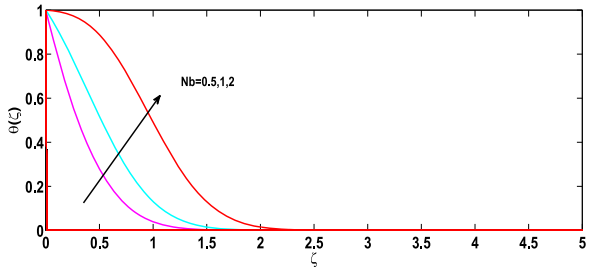

Fig. 12. Influence of *Nt* on temperature.

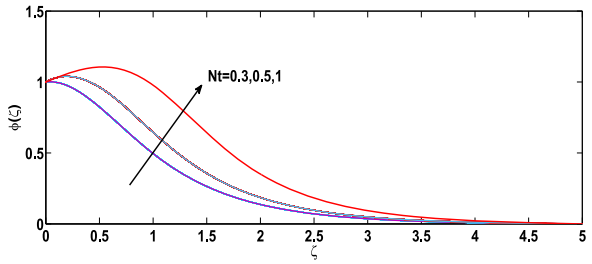

Fig. 13. Influence of *Nt* on concentration.

Concentration profiles

The effects of activation energy E, chemical reaction parameter γ thermophoresis parameter Nt and Brownian motion parameter Nb are described on concentration profiles through Figs. 13-–16. Fig. 13 portrays that species concentration gradually reduces as we keep on increasing the value of Brownian motion parameter Nb. Since Brownian diffusion rate is proportional to Nb, there is a downfall in the concentration. Fig. 14 depicts the behaviour of concentration profile φ upon strengthening the thermophoresis parameter Nt. This is due to migration of nano-particles from hotter region because of thermophoretic force and as a result of which we observe a downfall in concentration profile for magnetite nano-fluid. Fig. 15 demonstrates that as we gradually keep on increasing the chemical reaction parameter, a reduction in species concentration takes place. Basically, γ with a positive value indicates a chemical reaction of destructive nature. So, an increment in γ signifies consumption of species with a healthier rate. Consequently, a downfall in species

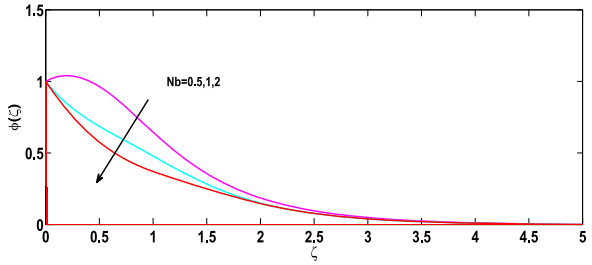

Fig. 14. Influence of *Nb* on concentration.

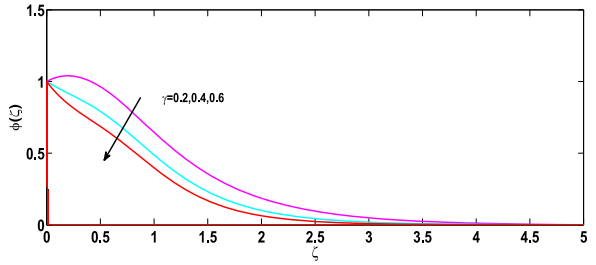

Fig. 15. Influence of γ on concentration.

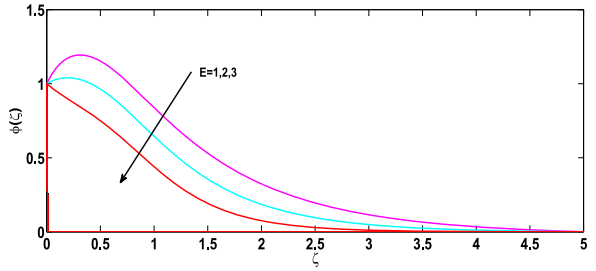

Fig. 16. Influence of E on concentration.

concentration is observed. With the help of the patterns of curves in Fig. 16 one can notice that higher the values of activation energy parameter E, lesser the concentration φ.This scenario can be supported with the fact that the key role of activation energy E is to improve the modified Arrhenius function $\frac{T}{T_\infty}^n \exp\left(\frac{E}{KT}\right)$, which ultimately works as a stimulator of the chemical reaction. As a result of which consumption of species occurs with a higher rate and naturally a reduction in φ is perceived.

Quantities of physical interest

In this section, we discuss the effects of porosity parameter λ, nanoparticle volume fraction ϕ and magnetic parameter M on the skin friction coefficient at the surface of disk through Figs. 17 and 18. Fig. 17 shows the variation of skin friction coefficient at the surface of disk for magnetic parameter M versus ϕ. Skin friction coefficient i.e $Re^{1/2}C_f$ has been enhanced for strengthening the nanoparticle volume fraction ϕ and same for magnetic parameter M as well. The impact of skin friction coefficient due to nanoparticle volume fraction and porosity parameter can be seen in Fig. 18. Here, we obtain enhancing values of $Re^{1/2}C_f$ for both Magnetic parameter M and porosity parameter λ. The rate of heat transfer i.e Nusselt number for thermophoresis parameter Nt and Brownian motion parameter Nb is displayed in Fig. 19. The decrement in the values of thermophoresis parameter Nt for rate of heat transfer takes place very slowly as we keep enhancing the value of Nt and same for Brownian motion Nb. Fig. 20 shows the variation of rate of mass transfer i.e Sherwood number for activation energy E versus Brownian motion Nb parameters. It can be seen from Fig. 20 that an increment in the values of Sherwood number for activation energy E takes place with the enhancement in the values of Nb and same phenomenon occurs for Brownian motion Nb.

7. Conclusions

The present study explains the effect of magnetite nanofluid flow past a porous rotating disk in the presence of magnetic field. The

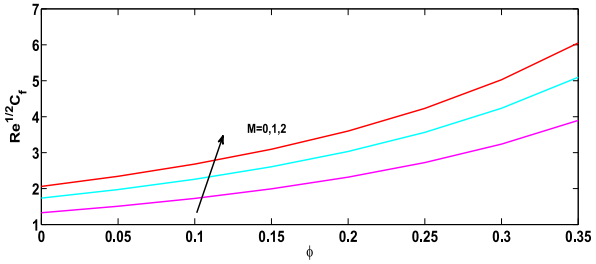

Fig. 17. Variation of skin friction coefficient for M versus ϕ.

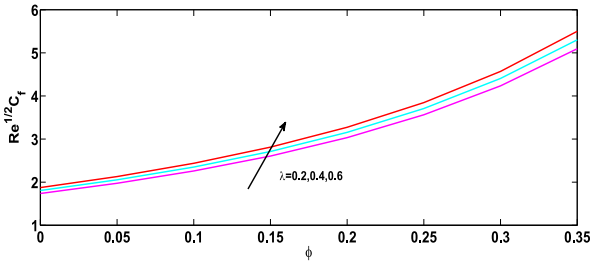

Fig. 18. Variation of skin friction coefficient for λ versus ϕ.

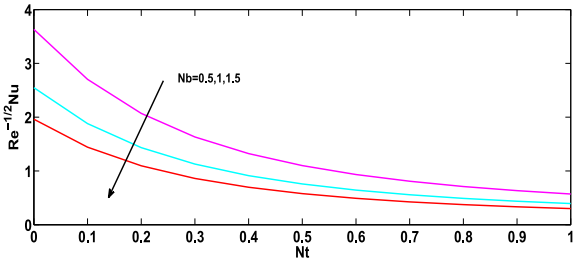

Fig. 19. Variation of Nusselt number for *Nb* versus *Nt*.

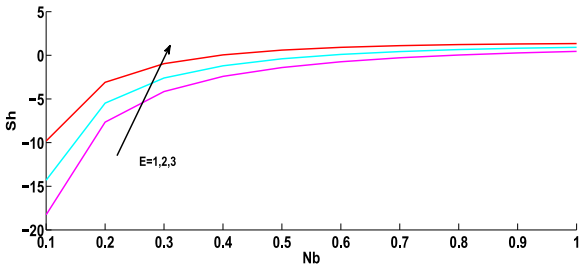

Fig. 20. Variation of Sherwood number for *E* versus *Nb*.

uniform temperature and concentration of the surface of the rotating disk are maintained at T_w and C_w, respectively, while the pressure, temperature and concentration of the ambient nanofluid are maintained at P_∞, T_∞ and C_∞, respectively. The impact of thermophoresis and Brownian motion are taken into consideration. Additionally, influence of chemical reaction between species, prompted by Arrhenius activation energy is considered into the model. The fourth order finite difference scheme is employed to solve the highly non-linear coupled ordinary differential equations. Significant outcomes are listed below:

- stronger magnitude of suction parameter W_s causes an increment in axial, radial and tangential velocity profiles.
- A downfall phenomenon is being observed in radial and tangential velocity profiles for nano-particle volume fraction ϕ, magnetic M and porosity parameters λ.
- An increment in *Nb* and *Nt* leads to an enhancement in temperature profile.
- Stronger thermophoresis parameter *Nt* yields an enhancement in concentration species whereas a reverse pattern is perceived for Brownian motion *Nb*, chemical reaction γ and activation energy parameter *E*.
- Skin friction coefficient at the surface of the disk gets increased for increasing values of magnetic parameter *M*, nanoparticle volume fraction ϕ and porosity parameter λ.
- Rate of heat transfer i.e. Nusselt number gets decreased for both parameters *Nb* and *Nt*.
- Sherwood number is being increased, for enhancing values of activation energy and Brownian motion parameters.

Declaration of Competing Interest

Authors confirm that the manuscript has not been published elsewhere and is not under consideration by another journal. All authors have approved the manuscript and agreed with the submission to Chinese Journal of Physics. Authors have read and abided by the statement of ethical standards for manuscripts submitted to Chinese Journal of Physics. The authors have no conflicts of interest to declare.

References

[1] H. Masuda, A. Ebata, K. Teramae, Alteration of thermal conductivity and viscosity of liquid by dispersing ultra-fine particles. dispersion of al2o3, sio2 and tio2 ultra-fine particles, Netsu Bussei 7 (4) (1993) 227–233.
[2] M. Mustafa, Mhd nanofluid flow over a rotating disk with partial slip effects: Buongiorno model, Int J Heat Mass Transf 108 (2017) 1910–1916.
[3] C. Yin, L. Zheng, C. Zhang, X. Zhang, Flow and heat transfer of nanofluids over a rotating disk with uniform stretching rate in the radial direction, Propul. Power Res. 6 (1) (2017) 25–30.
[4] Ç. Yıldız, M. Arıcı, H. Karabay, Comparison of a theoretical and experimental thermal conductivity model on the heat transfer performance of Al2O3-SiO2/water hybrid-nanofluid, Int J Heat Mass Transf 140 (2019) 598–605.
[5] H. Xu, Modelling unsteady mixed convection of a nanofluid suspended with multiple kinds of nanoparticles between two rotating disks by generalized hybrid model, Int. Commun. Heat Mass Transfer 108 (2019) 104275.
[6] R. Kumar, G. Seth, A. Bhattacharyya, Entropy generation of von karman's radiative flow with Al2O3 and Cu nanoparticles between two coaxial rotating disks: afinite-element analysis, The European Physical Journal Plus 134 (12) (2019) 597.
[7] K. Hosseinzadeh, S. Roghani, A. Asadi, A. Mogharrebi, D. Ganji, Investigation of micropolar hybrid ferrofluid flow over a vertical plate by considering various base fluid and nanoparticle shape factor, International Journal of Numerical Methods for Heat & Fluid Flow (2020), https://doi.org/10.1108/HFF-02-2020-0095.
[8] M. Gholinia, K. Hosseinzadeh, D. Ganji, Investigation of different base fluids suspend by CNTs hybrid nanoparticle over a vertical circular cylinder with sinusoidal radius, Case Studies in Thermal Engineering 21 (2020) 100666.
[9] I. Mustafa, T. Javed, A. Ghaffari, Heat transfer in MHD stagnation point flow of a ferrofluid over a stretchable rotating disk, J Mol Liq 219 (2016) 526–532.
[10] P. Lin, A. Ghaffari, Steady flow and heat transfer of the power-law fluid between two stretchable rotating disks with non-uniform heat source/sink, J Therm Anal Calorim (2020) 1–15, https://doi.org/10.1007/s10973-020-10142-x.
[11] K. Hosseinzadeh, S. Roghani, A. Mogharrebi, A. Asadi, M. Waqas, D. Ganji, Investigation of cross-fluid flow containing motile gyrotactic microorganisms and nanoparticles over a three-dimensional cylinder, Alexandria Engineering Journal 59 (5) (2020) 3297–3307.
[12] A. Rostami, K. Hosseinzadeh, D. Ganji, Hydrothermal analysis of ethylene glycol nanofluid in a porous enclosure with complex snowflake shaped inner wall, Waves Random Complex Medium (2020) 1–18, https://doi.org/10.1080/17455030.2020.1758358.
[13] G. Seth, R. Kumar, R. Tripathi, Thermo-diffusion effects on the magnetohydrodynamic natural convection flow of a chemically reactive brinkman type nanofluid in a porous medium, Bulgarian Chemical Communications 52 (2) (2019) 168–179.
[14] K. Pavlov, Magnetohydrodynamic flow of an incompressible viscous fluid caused by deformation of a plane surface, Magnitnaya Gidrodinamika 4 (1) (1974) 146–147.
[15] M. Rashidi, T. Hayat, E. Erfani, S.M. Pour, A.A. Hendi, Simultaneous effects of partial slip and thermal-diffusion and diffusion-thermo on steady mhd convective flow due to a rotating disk, Commun. Nonlinear Sci. Numer. Simul. 16 (11) (2011) 4303–4317.
[16] T. Hayat, M.W.A. Khan, M.I. Khan, M. Waqas, A. Alsaedi, Impact of chemical reaction in fully developed radiated mixed convective flow between two rotating disk, Physica B 538 (2018) 138–149.
[17] M.I. Khan, F. Shah, T. Hayat, A. Alsaedi, Transportation of cnts based nanomaterial flow confined between two coaxially rotating disks with entropy generation, Physica A 527 (2019) 121154.
[18] J. Ahmed, M. Khan, L. Ahmad, Transient thin film flow of nonlinear radiative maxwell nanofluid over a rotating disk, Phys. Lett. A 383 (12) (2019) 1300–1305.
[19] A. Bhat, N.N. Katagi, Micropolar fluid flow between a non-porous disk and a porous disk with slip: keller-box solution, Ain Shams Eng. J. 11 (1) (2020) 149–159.
[20] T. Hayat, M. Javed, M. Imtiaz, A. Alsaedi, Convective flow of jeffrey nanofluid due to two stretchable rotating disks, J Mol Liq 240 (2017) 291–302.
[21] J. Buongiorno, Convective transport in nanofluids, J Heat Transfer 128 (3) (2006) 240–250.
[22] K.U. Rehman, M. Malik, M. Zahri, M. Tahir, Numerical analysis of mhd casson navier's slip nanofluid flow yield by rigid rotating disk, Results Phys. 8 (2018) 744–751.
[23] M.H. Saidi, H. Tamim, Heat transfer and pressure drop characteristics of nanofluid in unsteady squeezing flow between rotating porous disks considering the effects of thermophoresis and brownian motion, Adv. Powder Technol. 27 (2) (2016) 564–574.
[24] Y. Lin, Y. Jiang, Effects of brownian motion and thermophoresis on nanofluids in a rotating circular groove: a numerical simulation, Int J Heat Mass Transf 123 (2018) 569–582.
[25] Z. Shah, T. Gul, S. Islam, M.A. Khan, E. Bonyah, F. Hussain, S. Mukhtar, M. Ullah, Three dimensional third grade nanofluid flow in a rotating system between parallel plates with brownian motion and thermophoresis effects, Results Phys. 10 (2018) 36–45.
[26] G. Seth, R. Kumar, A. Bhattacharyya, Entropy generation of dissipative flow of carbon nanotubes in rotating frame with Darcy-Forchheimer porous medium: anumerical study, J Mol Liq 268 (2018) 637–646.
[27] K. Hosseinzadeh, A. Asadi, A. Mogharrebi, M.E. Azari, D. Ganji, Investigation of mixture fluid suspended by hybrid nanoparticles over vertical cylinder by considering shape factor effect, J Therm Anal Calorim (2020) 1–15, https://doi.org/10.1007/s10973-020-09347-x.
[28] D. Kumar, K. Ramesh, S. Chandok, Mathematical modeling and simulation for the flow of magneto-powell-eyring fluid in an annulus with concentric rotating cylinders, Chin. J. Phys. 65 (2020) 187–197.
[29] G.S. Seth, R. Kumar, R. Tripathi, A. Bhattacharyya, Double diffusive MHD casson fluid flow in a non-darcy porous medium with newtonian heating and thermo-diffusion effects, Int. J. Heat Technol. 36 (4) (2018) 1517–1527.
[30] K. Hosseinzadeh, M.E. Moghaddam, A. Asadi, A. Mogharrebi, D. Ganji, Effect of internal fins along with hybrid nano-particles on solid process in star shape triplex latent heat thermal energy storage system by numerical simulation, Renew Energy 154 (2020) 497–507.
[31] J. Ahmed, M. Khan, L. Ahmad, Impact of nanoparticles and radiative heat flux in von kármán swirling flow of maxwell fluid, Chin. J. Phys. 62 (2019) 86–98.
[32] M. Sheikholeslami, M. Gorji-Bandpy, D.D. Ganji, P. Rana, S. Soleimani, Magnetohydrodynamic free convection of Al2O3-water nanofluid considering thermophoresis and brownian motion effects, Computers & Fluids 94 (2014) 147–160.
[33] T. Rafiq, M. Mustafa, M.A. Farooq, Numerical assessment of bödewadt flow and heat transfer over a permeable disk with variable fluid properties, Physica A 534 (2019) 122138.
[34] M.I. Khan, S. Qayyum, T. Hayat, M. Waqas, M.I. Khan, A. Alsaedi, Entropy generation minimization and binary chemical reaction with arrhenius activation energy in mhd radiative flow of nanomaterial, J Mol Liq 259 (2018) 274–283.
[35] K. Hosseinzadeh, D. Ganji, F. Ommi, Effect of SiO2 super-hydrophobic coating and self-rewetting fluid on two phase closed thermosyphon heat transfer characteristics: an experimental and numerical study, J Mol Liq 315 (2020) 113748.
[36] T. Hayat, S.A. Khan, M.I. Khan, A. Alsaedi, Theoretical investigation of ree–eyring nanofluid flow with entropy optimization and arrhenius activation energy between two rotating disks, Comput Methods Programs Biomed 177 (2019) 57–68.
[37] A. Kumar, R. Tripathi, R. Singh, Entropy generation and regression analysis on stagnation point flow of casson nanofluid with arrhenius activation energy, Journal of the Brazilian Society of Mechanical Sciences and Engineering 41 (8) (2019) 306.
[38] M. Rashidi, S. Abelman, N.F. Mehr, Entropy generation in steady MHD flow due to a rotating porous disk in a nanofluid, Int J Heat Mass Transf 62 (2013) 515–525.
[39] T. Hayat, M. Rashid, A. Alsaedi, Mhd convective flow of magnetite-fe3o4 nanoparticles by curved stretching sheet, Results Phys. 7 (2017) 3107–3115.
[40] B.V. Noumerov, A method of extrapolation of perturbations, Mon Not R Astron Soc 84 (1924) 592–601.
[41] M.K. Jain, Numerical Methods for Scientific and Engineering Computation, New Age International, 2003.
[42] E. Bogucz, J.D.A. Walker, Fourth-order finite-difference methods for two-point boundary-value problems, IMA J. Numer. Anal. 4 (1) (1984) 69–82.
[43] M. Turkyilmazoglu, Purely analytic solutions of magnetohydrodynamic swirling boundary layer flow over a porous rotating disk, Computers & Fluids 39 (5) (2010) 793–799.
[44] N. Kelson, A. Desseaux, Note on porous rotating disk flow, ANZIAM Journal 42 (2000) 837–855.